Macromolecules
ARTICLE

Macromolecules **2009**, *42*, 8969–8976 **8969**
DOI: 10.1021/ma901835n

Controllable Preparation and Optical Limiting Properties of POSS-Based Functional Hybrid Nanocomposites with Different Molecular Architectures

Xinyan Su,[†] Shanyi Guang,[†] Hongyao Xu,*[,†,‡] Xiangyang Liu,[§] Sheng Li,[†] Xin Wang,[†] Yan Deng,[⊥] and Pei Wang[⊥]

[†]*College of Material Science and Engineering & State Key Laboratory for Modification of Chemical Fibers and Polymer Materials, Donghua University, Shanghai 201620, China,* [‡]*State Key laboratory of Crystal Materials, Shandong University, Jinan 250100, China,* [§]*Department of Physics, National University of Singapore, 117542, Singapore, and* [⊥]*Department of Physics, University of Science and Technology of China, Hefei 230026, China*

Received August 17, 2009; Revised Manuscript Received October 6, 2009

ABSTRACT: A series of soluble polyhedral oligomeric silsesquioxane (POSS) based inorganic−organic hybrid nonlinear optical materials with different architectures, such as dumbbell-type, bead-type and network-type structure, were prepared based on the hydrosilylation addition reaction of multifunctional octahydridosilsesquioxane ($\mathbf{T_8^H}$) with different azobenzene chromophore monomers. These resultant hybrid composites are soluble in common organic solvents such as tetrahydrofuran, toluene, and chloroform, and exhibit good film-forming ability. Their structures and properties were characterized and evaluated with IR, ^{1}H NMR, ^{29}Si NMR, TGA, DSC, optical limiting measurement and Z-scan technique, respectively. The results show that the structure of these resultant hybrids can be effectively tuned by simply varying the feed ratio and molecular structure of organic chromophore monomers. The incorporation of inorganic POSS into organic azobenzene chromophore has endowed the hybrids with well optical limiting properties and high thermal stability. Simultaneously, the relationship between molecular structure and properties of these hybrids were investigated in detail.

Introduction

With the repaid development of new lasers and laser technology, the optical limiting (OL) materials have attracted great interest in recent years due to the growing needs for protection of human eyes and optical sensors from laser damage in both civilian and military applications. The π-conjugated organic nonlinear optical (NLO) materials, including stilbenes,[1] azobezenes,[2] fullerenes (C_{60}),[3] carbon nanotubes,[4] phthalocyanines,[5] porphyrins,[6] and organometallic compounds[7] are considered to be promising materials owing to their fast response time, high damage threshold, ease of structure modification, and their application over a wide range of wavelength. However, the easy crystallization, poor solubility and processability, and low thermal stability have limited their application in the devices as limiters. Thus, how to improve the processability and thermal stability of these OL materials will be very significant for practical application.

Organic/inorganic hybrids have drawn great attention recently because of their better performance in thermal stability and oxidative resistance compared to their mother homogeneous organic materials due to the combination of the functional versatility of organic compounds with the advantage in thermal stability of inorganic substrates. A typical hybrid material will contain an organic phase bound covalently with inorganic moieties, in which inorganic particles act as a key structural component.[8] Nevertheless, the major difficulty encountered during the materials preparation is how to bind an organic compound covalently with inorganic moieties. Over the past decade, these synthetic difficulties have been gradually overcome due to the discovery of the polyhedral oligomeric silsesquoixanes macromer (POSS) with a well-defined structure, which has a cube-like inorganic core (Si_8O_{12}) surrounded by eight organic corner groups (functional or inert).[9−11] In particular, these POSSs are cubeoctameric molecules of nanoscale dimensions (0.5−3 nm), which are excellent platforms and blocks for nanotechnology applications and architecture of novel organic/inorganic hybrid materials.[12,13] The aggregation effect is effectively overcome owing to the chemically incorporation of POSS at molecular level in these hybrid materials, which often occurs in other hybrid composites prepared by simple physical mixture.[12] POSS-based hybrid materials have received much attention recently among the materials science community and industry application fields. By incorporating POSS cages into organic molecules or polymers, the superior properties of the resultant material such as thermal and mechanical properties,[13−16] adhesion[17] and dielectric properties have been realized.[18] Many POSS-based functional materials, such as liquid crystal (LC) materials,[19,20] light-emitting materials,[21−26] dental restorative materials,[27] and degradable polymeric biomaterials[28] have been prepared. Our group has also reported a series of POSS-containing hybrid materials, their controllable preparation and properties, and found that these hybrid materials possess superior thermal properties and good solubility.[29−32] However, the systematically investigation on architecture and controllable preparation of functional POSS-based hybrids with optical limiting properties, so far, are seldom reported.[33,34]

In this work, we designed and synthesized a series of novel soluble functional hybrids with different architectures such as

*Corresponding author. Telephone: +86-21-67792874. E-mail: hongyaoxu@163.com.

Published on Web 10/14/2009

Scheme 1. Synthetic Routes of Monomer Molecules

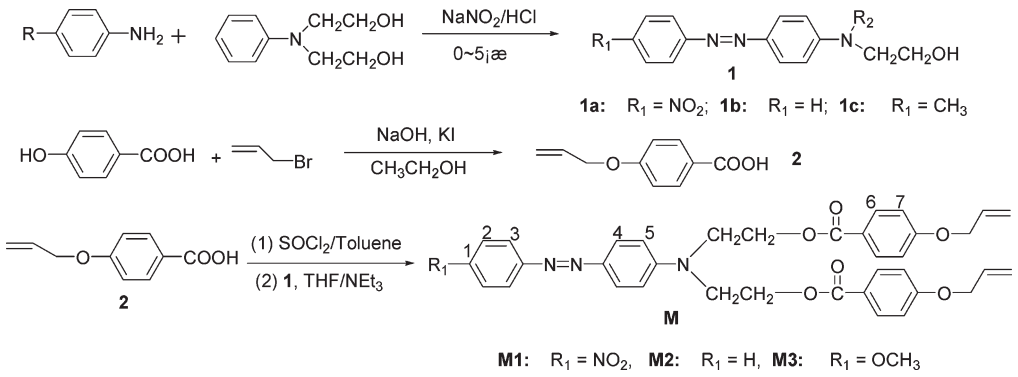

Scheme 2. Synthetic Routes to the Hybrids

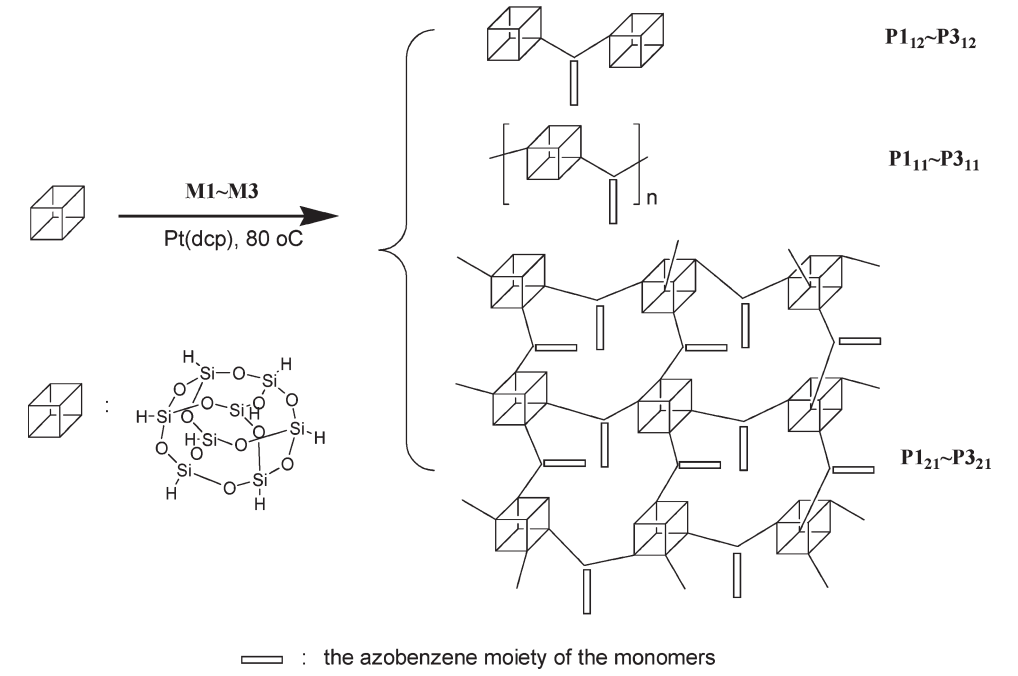

dumbbell-type, bead-type or network-type structure, based on the hydrosilylation addition method between octahydridosilsesquioxane ($\mathbf{T_8^H}$) and different azobenzene chromophore monomers (Schemes 1 and 2). Their optical limiting properties and the relationship between molecular structure and properties were systematically investigated.

Experimental Section

Materials. *N*,*N*-Bis(2-hydroxyethyl)aniline and allyl bromide were purchased from Aldrich. Aniline, 4-methoxyaniline, 4-nitroaniline, and 4-hydroxybenzoic acid were purchased from Shanghai Chemical Reagent Company. Dioxane, THF, and toluene were distilled from sodium benzophenone ketyl immediately prior to use. Triethylamine was distilled from potassium hydroxide prior to use.

Octahydridosilsesquioxane ($\mathbf{T_8^H}$) was synthesized according to the procedures described in ref.[35] Platinum dicyclopentadiene complex, Pt(dcp), was synthesized by the literature procedures.[36,37] Platinum divinyltetramethyldisiloxane complex, Pt(dvs), was obtained from PCR Co. and diluted to a 2 mM solution in distilled toluene before use.

Instruments. The IR spectra were recorded as KBr pellets on a Nicolet 170sx spectrometer. ^{1}H NMR and ^{29}Si NMR spectra were collected on an AVANCE/DMX-500 MHz Bruker NMR spectrometer. Tetramethylsilane was used as the internal reference for the ^{1}H NMR analyses. The cross-polarization method was performed to obtain the solid-state ^{29}Si MAS NMR spectra. UV−vis spectra were recorded on a Shimadzu UV-265 spectrometer using a 1 cm square quartz cell. Differential scanning calorimetry (DSC) was performed on a TA Instruments DSC 9000 equipped with a liquid nitrogen cooling accessory (LNCA) unit under a continuous nitrogen purge (50 mL/min). The scan rate was 10 °C/min within the temperature range 30−300 °C. Thermal analyses of the polymers were performed on a Perkin-Elmer TGA (Thermogravimetric analysis) under nitrogen at a heating rate of 10 °C/min. Molecular weights of the polymers were estimated by a Waters associates gel permeation chromatography (GPC) using 12 monodisperse polystyrenes (molecular weight range 10^2-10^7) as calibration standards. The sample solutions were prepared in THF (ca. 2 mg/mL) and filtered through 0.45-um poly(tetrafluoroethylene) syringe-type filters before injected into the GPC system.

The investigation of the optical limiting properties of the samples was carried out by using a frequency doubled, Q-switched, mode-locked Continuum ns/ps Nd:YAG laser, which provides linearly polarized 13 ns optical pulses at 532 nm wavelength with a repetition of 1 Hz. The experimental arrangement is similar to that in the literature.[38] The samples

were housed in quartz cells with a path of 2 mm. The input laser pulses adjusted by an attenuator (Newport) were split into two beams. One was employed as a reference to monitor the incident laser energy, and the other was focused onto the sample cell by using a lens with a 300 mm focal length. The samples were positioned at the focus. The incident and transmitted laser pulses were monitored by two energy detectors, D1 and D2 (Rjp-735 energy probes, Laser Precision).

The nonlinear optical properties of the samples were performed by a Z-scan technique with the laser system as in the optical limiting experiment. The experiment was set up as in the literature.[39] The solution sample was contained in a 2 mm quartz cell. The input energy was 40 μJ. The radius ω_0 at beam waist was 70 mm. The samples were moved along the axis of the incident beam (z direction). The experimental data were collected utilizing a single shot at a rate of 1 pulse/min to avoid the influence of thermal effect.

Monomer Synthesis. *2,2′-(4-((4-Nitrophenyl)diazenyl)phenylazanediyl)diethanol* (***1a***). 4-Nitroaniline (6.91 g, 50 mmol) was dissolved in 20 mL concentrated hydrochloric acid. After cooling to 0 °C, an ice−water solution of sodium nitrite (3.45 g, 50 mmol) was added dropwise and stirred for 30 min. The mixture was then added dropwise to an buffered aqueous solution (acetic acid/sodium acetate, pH ≈ 6) containing *N, N*-bis(2-hydroxyethyl)aniline (9.42 g, 52 mmol) and stirred for 2 h at 0−5 °C. The resulting precipitate was filtered and rinsed twice with water. The crude product was recrystallized twice from ethanol to provide red crystals in 91% yield. mp 177 °C. IR (KBr), υ (cm^{-1}): 3427 (OH), 2968, 2868 (CH_3, CH_2), 1598, 1512 (Ar), 1423 (−*N*═N−), 1335 (NO_2). ^{1}H NMR (500 MHz, $CDCl_3$), δ (TMS, ppm): 3.32 (t, J = 4.5 Hz, 4H, C$H_2$$CH_2$OH), 3.61 (t, 4H, CH_2CH_2OH), 6.91 (d, J = 8.7 Hz, 2H, H^5), 7.83 (d, 2H, H^4), 7.93 (d, J = 8.7 Hz, 2H, H^3), 8.36 (d, 2H, H^2). Anal. Calcd for $C_{16}H_{18}N_4O_4$: C 58.17; H 5.49; N 16.96. Found: C 58.34; H 5.41; N 16.87.

2,2′-(4-(Phenyldiazenyl)phenylazanediyl)diethanol (***1b***). This was prepared as above from aniline and *N,N*-bis(2-hydroxyethyl)aniline. The crude product was recrystallized from ethanol twice to give red crystals in 89% yield. mp 181 °C. IR (KBr), υ (cm^{-1}): 3455 (OH), 2939, 2893 (CH_3, CH_2), 1598, 1513 (Ar), 1432 (−*N*═N−). ^{1}H NMR (500 MHz, $CDCl_3$), δ (TMS, ppm): 3.74 (t, J = 4.8 Hz, 4H, C$H_2$$CH_2$OH), 3.96 (t, 4H, CH_2CH_2OH), 6.84 (d, J = 9.0 Hz, 2H, H^5), 7.39 (t, J = 7.5 Hz, 1H, H^1), 7.48 (d, J = 7.8 Hz, 2H, H^2), 7.88 (m, 4H, $H^{3,4}$). Anal. Calcd for $C_{16}H_{19}N_3O_2$: C 67.35; H 6.71; N 14.73. Found: C 67.74; H 6.54; N 14.59.

2,2′-(4-((4-Methoxyphenyl)diazenyl)phenylazanediyl)diethanol (***1c***). This was prepared as above from 4-methoxyaniline and *N,N*-bis(2-hydroxyethyl)aniline. The crude product was recrystallized from ethanol twice to give yellow crystals in 92% yield. mp 185 °C. IR (KBr), υ (cm^{-1}): 3427 (OH), 2960, 2868 (CH_3, CH_2), 1597, 15136 (Ar), 1426 (−*N*═N−), 1246 (C−O−C). ^{1}H NMR (500 MHz, $CDCl_3$), δ (TMS, ppm): 3.70 (t, J = 4.5 Hz, 4H, C$H_2$$CH_2$OH), 3.93 (m, 7H, CH_2CH_2OH and CH_3O), 6.78 (d, J = 8.4 Hz, 2H, H^5), 6.98 (d, J = 9.0 Hz, 2H, H^2), 7.84 (m, 4H, $H^{3,4}$). Anal. Calcd for $C_{17}H_{21}N_3O_3$: C 64.74; H 6.71; N 13.32. Found: C 64.13; H 6.58; N 13.14.

4-(Allyloxy)benzoic acid (***2***). Sodium hydroxide (2.0 g, 0.05 mol) was added to a solution of 4-hydroxybenzoic acid (6.91 g, 0.05 mol) in 50 mL of ethanol. After the reaction mixture was stirred at room temperature for 1 h, allyl bromide (7.26 g, 0.06 mol) was added dropwise to the mixture. The resulting mixture was heated under reflux overnight. After this had cooled to room temperature, 1 mol/L HCl solution was added to neutralize the reaction mixture. The white precipitate was filtered and recrystallized from ethanol twice to give white piece crystals in 75% yield. IR (KBr), υ (cm^{-1}): 2924, 2852 (CH_3, CH_2), 1680 (*C* = O), 1580,1500 (Ar), 1250 (C−O−C). ^{1}H NMR (500 MHz, $CDCl_3$), δ (TMS, ppm): 4.6 (d, 2H, OCH_2CH), 5.4 (m, 2H, CH═CH_2), 6.09 (m, 1H, C*H*═CH_2), 6.98 (d, J = 6.9 Hz, 2H, Ar−H), 8.07 (d, 2H, Ar−H). Anal. Calcd for $C_{10}H_{10}O_3$: C 67.41; H 5.66. Found: C 67.32; H 5.48.

2,2′-(4-((4-Nitrophenyl)diazenyl)phenylazanediyl)bis(ethane-2,1-diyl) Bis(4-(allyloxy)benzoate) (***M1***). In a two-necked, 250 mL, round-bottom flask under nitrogen were dissolved of **2** (3.56 g, 0.02 mol) and 2 mL of $SOCl_2$ in 60 mL of anhydrous toluene. The mixture was refluxed at 80 °C for 5 h. The solvent and excessive $SOCl_2$ were removed under reduced pressure, and the residue was dissolved in 40 mL anhydrous THF with 3 mL anhydrous Et_3N. The solution was cooled to 0 °C, and then **1a** (6.60 g, 0.02 mol) was added. After 12 h of refluxing, the solvent was removed under reduced pressure, and the crude product was purification by recrystallization from THF, monomer **M1** was obtained as red crystals in 81% yield. mp 170 °C. IR (KBr), υ (cm^{-1}): 2942 (CH_2), 1702(*C* = O), 1602, 1514 (Ar), 1459 (-*N* = N-), 1335 (NO_2). ^{1}H NMR (500 MHz, $CDCl_3$), δ (TMS, ppm): 3.95 (t, J = 5.7 Hz, 4H, NC$H_2$$CH_2$O), 4.58 (m, 8H, NCH_2CH_2O and OCH_2CH), 5.31 (d, J = 10.5 Hz, 2H, CH═CH_2), 5.42 (d, J = 17.4 Hz, 2H, CH═CH_2), 6.04 (m, 2H, C*H*═CH_2), 6.93 (d, J = 8.7 Hz, 2H, H^5), 6.99 (d, J = 8.7 Hz, 4H, H^7), 7.97 (m, 8H, $H^{3,4,6}$), 8.35 (d, J = 8.1 Hz, 2H, H^2). Anal. Calcd for $C_{36}H_{34}N_4O_8$: C 66.45; H 5.27; N 8.61. Found: C 66.46; H 5.28; N 8.69.

2,2′-(4-(Phenyldiazenyl)phenylazanediyl)bis(ethane-2,1-diyl) Bis(4-(allyloxy)benzoate) (***M2***). This was prepared as above from **2** and **1b**. Monomer M2 was obtained as yellow crystals in 86% yield. mp 173 °C. IR (KBr), υ (cm^{-1}): 2921 (CH_2), 1713(*C*═O), 1605, 1511 (Ar), 1457 (−*N*═N−). ^{1}H NMR (500 MHz, $CDCl_3$), δ (TMS, ppm): 3.90 (t, J = 6.0 Hz, 4H, NC$H_2$$CH_2$O), 4.53 (t, 4H, NCH_2CH_2O), 4.55 (d, J = 2.1 Hz, 4H, OCH_2CH), 5.28 (d, J = 10.5 Hz, 2H, CH═CH_2), 5.39 (d, J = 17.4 Hz, 2H, CH═CH_2), 5.98 (m, 2H, C*H*═CH_2), 6.88 (d, J = 9.0 Hz, 2H, H^5), 6.95 (d, J = 8.7 Hz, 4H, H^7), 7.37 (t, J = 8.7 Hz, 1H, H^1), 7.45 (d, J = 8.7 Hz, 2H, H^2), 7.94 (m, 8H, $H^{3,4,6}$). Anal. Calcd for $C_{36}H_{35}N_3O_6$: C 71.39; H 5.82; N 6.94. Found: C 72.35; H 5.78; N 6.97.

2,2′-(4-((4-Methoxyphenyl)diazenyl)phenylazanediyl)bis(ethane-2,1-diyl) Bis(4-(allyloxy)benzoate) (***M3***). This was prepared as above from **2** and **1c**. Monomer **M3** was obtained as yellow crystals in 84% yield. mp 176 °C. IR (KBr), υ (cm^{-1}): 2923 (CH_2), 1715(*C*═O), 1603, 1512 (Ar), 1445 (−*N*═N−), 1254 (C−O−C). ^{1}H NMR (500 MHz, $CDCl_3$), δ (TMS, ppm): 3.90 (t, 7H, NC$H_2$$CH_2$O and CH_3O), 4.52 (t, J = 6.0 Hz, 4H, NCH_2CH_2O), 4.57 (d, J = 3.9 Hz, 4H, OCH_2CH), 5.31 (d, J = 10.5 Hz, 2H, CH═CH_2), 5.35 (d, J = 17.1 Hz, 2H, CH═CH_2), 6.01 (m, 2H, C*H* = CH_2), 6.92 (m, 6H, $H^{5,7}$), 6.97 (d, J = 6.0 Hz, 2H, H^2), 7.88 (m, 8H, $H^{3,4,6}$). Anal. Calcd for $C_{37}H_{37}N_3O_7$: C 69.91; H 5.87; N 6.61. Found: C 69.96; H 5.89; N 6.59.

Synthesis of POSS-Based Hybrids. The POSS-based hybrids $\mathbf{P}\boldsymbol{n}_{\boldsymbol{xy}}$, in which ***n*** denotes different monomer, **x** and **y** express the molar feed ratio of chromophore monomer (***x***) to POSS (***y***), were prepared by a conventional hydrosilylation addition reactions using Pt(dcp) as a catalyst, as shown in Scheme 2. The hydrosilylation reactions were carried out under nitrogen using a vacuum-line system. Taking synthesis of dumbbell-type structural hybrid $\mathbf{P1_{12}}$ as an example: **M1** (32.6 mg, 0.05 mmol) in 5 mL of dioxane is added dropwise into $\mathbf{T_8^H}$ (42.4 mg, 0.1 mmol) and 1.0 mg of Pt(dcp) dioxane solution in a 25 mL Schlenk flask. Then, the mixture was stirred at 80 °C for 10 h under nitrogen. The reaction was monitored by TLC and ^{1}H NMR. On reaction completion, the reaction mixture was precipitated into 100 mL of hexane under vigorously agitation. The precipitate was collected by filtration and redissolved in minimal THF. The THF solution was added dropwise into 100 mL of hexane to precipitate the hybrids. This purification procedure was repeated three times. Other hybrids were prepared by similar method.

P1$_{12}$. Red powder. M_n = 1720, PDI, 1.20, (GPC, polystyrene). Yield: 47%. IR (KBr), υ (cm^{-1}): 2926, 2848 (CH_3, CH_2), 2254 (Si−H), 1705 (*C*═O), 1615, 1514 (Ar), 1336 (NO_2),

1121(Si−O−Si). ^{1}H NMR (500 MHz, $CDCl_3$), δ (TMS, ppm): 0.68 (br, CH_2CH_3CHSi), 0.86 (br, CH_2CH_2Si), 1.27 (br, CH_2CH_3CHSi), 1.86 (br, CH_2CH_2Si), 3.92 (br, 8H, NCH_2CH_2O and $CH_2CH_2CH_2Si$), 4.16 (br, SiH), 4.56 (br, 4H, NCH_2CH_2O), 6.87 (br, 6H, Ar−H), 7.93 (br, 8H, Ar−H), 8.29 (br, 2H, Ar−H). ^{29}Si NMR (79.49 MHz; solid), δ (ppm): −64.58 (s, Si−C), −83.32 (s, Si−H).

P2$_{12}$. Yellow powder. M_n = 1610, PDI, 1.24 (GPC, polystyrene). Yield: 61%. IR (KBr), υ (cm^{-1}): 2947, 2879 (CH_3, CH_2), 2254 (Si−H), 1713 (C=O), 1602, 1513 (Ar), 1138 (Si−O−Si). ^{1}H NMR (500 MHz, $CDCl_3$), δ (TMS, ppm): δ 0.67 (br, CH_2CH_3CHSi), 0.86 (br, CH_2CH_2Si), 1.22 (br, CH_2CH_3CHSi), 1.85 (br, CH_2CH_2Si), 3.86 (br, 8H, NCH_2CH_2O and $CH_2CH_2CH_2Si$), 4.21 (br, SiH), 4.53 (br, 4H, NCH_2CH_2O), 6.91 (br, 4H, Ar−H), 7.46 (br, 3H, Ar−H), 7.88 (br, 8H, Ar−H). ^{29}Si NMR (79.49 MHz; solid), δ (ppm): −64.51 (s, Si−C), −83.35 (s, Si−H).

P3$_{12}$. Yellow powder. M_n = 1680, PDI, 1.22 (GPC, polystyrene). Yield: 49%. IR (KBr), υ (cm^{-1}): 2923, 2859 (CH_3, CH_2), 2254 (Si−H), 1707 (C=O), 1604, 1513 (Ar), 1253 (CH_3O), 1121 (Si−O−Si). ^{1}H NMR (500 MHz, $CDCl_3$), δ (TMS, ppm): 0.67 (br, CH_2CH_3CHSi), 0.87 (br, CH_2CH_2Si), 1.26 (br, CH_2CH_3CHSi), 1.85 (br, CH_2CH_2Si), 3.88 (br, 11H, NCH_2CH_2O, $CH_2CH_2CH_2Si$ and CH_3O), 4.17 (br, SiH), 4.53 (br, 4H, NCH_2CH_2O), 6.87 (br, 6H, Ar−H), 6.97 (br, 2H, Ar−H), 7.93 (br, 8H, Ar−H). ^{29}Si NMR (79.49 MHz; solid), δ (ppm): −64.85 (s, Si−C), −83.21 (s, Si−H).

P1$_{11}$. Red powder. M_n = 6890, PDI, 1.30 (GPC, polystyrene). Yield: 54%. IR (KBr), υ (cm^{-1}): 2922, 2851 (CH_3, CH_2), 2254 (Si−H), 1706 (C=O), 1615, 1514 (Ar), 1336 (NO_2), 1121(Si−O−Si). ^{1}H NMR (500 MHz, $CDCl_3$), δ (TMS, ppm): 0.67 (br, CH_2CH_3CHSi), 0.86 (br, CH_2CH_2Si), 1.25 (br, CH_2CH_3CHSi), 1.85 (br, CH_2CH_2Si), 3.91 (br, 8H, NCH_2CH_2O and $CH_2CH_2CH_2Si$), 4.16 (br, SiH), 4.54 (br, 4H, NCH_2CH_2O), 6.86 (br, 6H, Ar−H), 7.93 (br, 8H, Ar−H), 8.28 (br, 2H, Ar−H). ^{29}Si NMR (79.49 MHz; solid), δ (ppm): −64.61 (s, *Si*-C), −83.31 (s, Si−H).

P2$_{11}$. Yellow powder. M_n = 6650, PDI, 1.25 (GPC, polystyrene). Yield: 57%. IR (KBr), υ (cm^{-1}): 2947, 2879 (CH_3, CH_2), 2254 (Si−H), 1713 (C=O), 1602, 1513 (Ar), 1138 (Si−O−Si). ^{1}H NMR (500 MHz, $CDCl_3$), δ (TMS, ppm): 0.67 (br, CH_2CH_3CHSi), 0.86 (br, CH_2CH_2Si), 1.24 (br, CH_2CH_3CHSi), 1.86 (br, CH_2CH_2Si), 3.87 (br, 8H, NCH_2CH_2O and $CH_2CH_2CH_2Si$), 4.21 (br, SiH), 4.52 (br, 4H, NCH_2CH_2O), 6.92 (br, 4H, Ar−H), 7.47 (br, 3H, Ar−H), 7.88 (br, 8H, Ar−H). ^{29}Si NMR(79.49 MHz; solid), δ (ppm): −64.49 (s, Si−C), −83.30 (s, Si−H).

P3$_{11}$. Yellow powder. M_n = 6780, PDI, 1.27 (GPC, polystyrene). Yield: 46%. IR (KBr), υ (cm^{-1}): 2923, 2859 (CH_3, CH_2), 2254 (Si−H), 1707 (C=O), 1604, 1513 (Ar), 1253 (CH_3O), 1121 (Si−O−Si). ^{1}H NMR (500 MHz, $CDCl_3$), δ (TMS, ppm): 0.67 (br, 3H, CH_2CH_3CHSi), 0.86 (br, 3H, CH_2CH_2Si), 1.25 (br, 3H, CH_2CH_3CHSi), 1.85 (br, 3H, CH_2CH_2Si), 3.86 (br, 11H, NCH_2CH_2O, $CH_2CH_2CH_2Si$ and CH_3O), 4.17 (br, SiH), 4.51 (br, 4H, NCH_2CH_2O), 6.83 (br, 6H, Ar−H), 6.95 (br, 2H, Ar−H), 7.92 (br, 8H, Ar−H). ^{29}Si NMR (79.49 MHz; solid), δ (ppm): −64.97 (s, Si−C), −83.34 (s, Si−H).

P1$_{21}$. Red powder. M_n = 11900, PDI, 1.28 (GPC, polystyrene). Yield: 42%. FTIR (KBr), υ (cm^{-1}): 2924, 2857 (CH_3, CH_2), 2254 (Si−H), 1713 (C=O), 1610, 1512 (Ar), 1335 (NO_2), 1121 (Si−O−Si). ^{1}H NMR (500 MHz, $CDCl_3$), δ (TMS, ppm): 0.67 (br, CH_2CH_3CHSi), 0.85 (br, CH_2CH_2Si), 1.26 (br, CH_2CH_3CHSi), 1.85 (br, CH_2CH_2Si), 3.91 (br, 8H, NCH_2CH_2O and $CH_2CH_2CH_2Si$), 4.17 (br, SiH), 4.56 (br, 4H, NCH_2CH_2O), 6.86 (br, 6H, Ar−H), 7.91 (br, 8H, Ar−H), 8.27 (br, 2H, Ar−H). ^{29}Si NMR (79.49 MHz; solid), δ (ppm): −65.01 (s, Si−C), −83.42 (s, Si−H).

P2$_{21}$. Yellow powder. M_n = 11380, PDI, 1.22 (GPC, polystyrene). Yield: 48%. IR (KBr), υ (cm^{-1}): 2947, 2879 (CH_3, CH_2), 2254 (Si−H), 1713 (C=O), 1602, 1513 (Ar), 1138 (Si−O−Si). ^{1}H NMR (500 MHz, $CDCl_3$), δ (TMS, ppm): 0.68 (br, CH_2CH_3CHSi), 0.86 (br, CH_2CH_2Si), 1.26 (br, CH_2CH_3CHSi), 1.86 (br, CH_2CH_2Si), 3.87 (br, 8H, NCH_2CH_2O and $CH_2CH_2CH_2Si$), 4.20 (br, SiH), 4.52 (br, 4H, NCH_2CH_2O), 6.92 (br, 4H, Ar−H), 7.47 (br, 3H, Ar−H), 7.87 (br, 8H, Ar−H). ^{29}Si NMR (79.49 MHz; solid), δ (ppm): −65.11 (s, Si−C), −83.46 (s, Si−H).

P3$_{21}$. Yellow powder. M_n = 11640, PDI, 1.31 (GPC, polystyrene). Yield: 44%. IR (KBr), υ (cm^{-1}): 2923, 2859 (CH_3, CH_2), 2254 (Si−H), 1707 (C=O), 1604, 1513 (Ar), 1253 (CH_3O), 1121 (Si−O−Si). ^{1}H NMR (500 MHz, $CDCl_3$), δ (TMS, ppm): 0.67 (br, CH_2CH_3CHSi), 0.84 (br, CH_2CH_2Si), 1.26 (br, CH_2CH_3CHSi), 1.87 (br, CH_2CH_2Si), 3.88 (br, 11H, NCH_2CH_2O, $CH_2CH_2CH_2Si$ and CH_3O), 4.17 (br, SiH), 4.52 (br, 4H, NCH_2CH_2O), 6.85 (br, 6H, Ar−H), 6.94 (br, 2H, Ar−H), 7.92 (br, 8H, Ar−H). ^{29}Si NMR (79.49 MHz; solid), δ (ppm): −65.11 (s, Si−C), −83.46 (s, Si−H).

Results and Discussion

Monomer Synthesis. We designed and synthesized three different bis(allyloxy)azobenzene chromophore monomers (**M1**−**M3**, Scheme 1) with different terminal substituted group (H, OCH_3 and NO_2). The diazotization-coupling reaction of these different aniline derivatives with *N*,*N*-bis-(2-hydroxyethyl)aniline gave azobenzene derivative **1a**−**1c**. 4-Hydroxybenzoic acid was etherized with allyl bromide to give 4-(allyloxy)benzoic acid (**2**). Treatment of **2** with thionyl chloride, followed by a reaction with **1** (**1a**−**1c**) gave the objective monomers (**M1**−**M3**) in high yields.

Preparation of Hybrids. The hybrids are prepared via hydrosilylative addition reaction between the Si−H groups of cube-like polyhedral oligomeric silsesquioxanes (POSS) and the bis(allyoxy)azobenzene chromophore monomers (**M1**−**M3**) (Scheme 2), in which POSSs are covalently incorporated into hybrids. During the synthesis of hydrosilylation reactions of objective POSS-based hybrids, two catalysts, Pt(dvs) and Pt(dcp), were attempted, respectively. The results display that hydrosilylation reactions catalyzed by Pt(dvs) only gave cross-linked gels with low yields or partially soluble products. However, soluble products in moderate yield were obtained by using Pt(dcp) as a catalyst.

To detect the structure of resulting products, we had once tried to use LC−MS method to separate and verify the structure of the products such as dumbbell-type hybrid **P1$_{12}$**. LC−MS results indicated a small amount of the various substituted POSS (ca. 2−5 wt %) existed in the resulting product besides main dumbbell-type hybrid **P1$_{12}$** (more than 90 wt %). Simultaneously, it was found that a little cross-linked byproduct (less than 2 wt %) in our resultant product still retained in the chromatogram column and badly contaminated the chromatogram system, which destroyed the ordinal work of LC−MS equipment, also hinting that it is difficult that the products are separated and evaluated by chromatographic method.

Therefore, we evaluated the resultant hybrid using GPC method in the work. However, for protecting the gel permeation chromatography system, the resultant sample solutions (ca. 2 mg/mL) were filtered through 0.45-um poly(tetrafluoroethylene) syringe-type filters before injected into the GPC system. Therefore, the structures of the resulting hybrids are deduced by GPC and spectral method.

Thus, we investigated the hydrosilylative addition reaction between the bis-allyoxy monomers (***x***) and POSS molecules (***y***) by varying the feed ratio (***x***:***y***). It is found that main dumbbell-type structural hybrids were obtained when ***x***:***y*** is 1:2. Similarly, the 1:1 molar feed ratio to mainly give bead-type structural hybrid composites while the network-type

structural hybrids were mainly obtained at higher feed ratio (x:y, y = 1, x = 2, 3, or 4). The structure of the hybrids can be deduced by GPC and spectral method. For examples, the average molecular weight (M_n) and polydispersity index (PDI) estimated from GPC are 1720 and 1.20 for **P1$_{12}$** while calculated molecular weight is ca. 1500 for dumbbell-type structural hybrid (**P1$_{12}$**) and lower than result obtained from GPC measurement, which may be due to the structural difference between the hybrids and standard polystyrenes for GPC measurement and existent small amount of un-dumbbell-type structural hybrids. Simultaneously, it is found that **P1$_{12}$** hybrids are completely soluble in common solvent such as tetrahydrofuran, toluene, and chloroform, further supporting **P1$_{12}$** molecules may be mainly dumbbell-type structural hybrid. Similar phenomenon is found in bead-type structural **P1$_{11}$** composites, which the average molecular weight (M_n) and polydispersity index (PDI) are 6980 and 1.30. However, when the feed ratio of chromophore monomer (x) to POSS (y) is 2:1, the solubility of the resulting hybrids decreases and **P1$_{21}$** is only part soluble in the above solvents, hinting the cross-linked structure was formed. When the feed ratio is at 3:1 or 4:1, the resultant hybrids are almost completely insoluble in all common organic solvent, which may be owing to formation of high cross-linked network-type structure, suggesting that the hybrids with different architecture may be effectively adjusted by varying the feed ratio.

Structural Characterization. Figure 1 shows the IR spectra of **M1** and the hybrids (**P1**$_{xy}$). For comparison, the spectrum of POSS (**T$_8^H$**) is also given in the same figure. As shown in Figure 1, **M1** shows a characteristic band at 1702 cm^{-1} for the carbonyl stretching vibration of the ester group. T$_8^H$ shows three characteristic peaks at 2265 (Si−H stretching), 1120 (Si−O−Si stretching), and 860 cm^{-1} (Si−H bending). The intensity of Si−H characteristic absorption bands obviously decreases in the IR spectrum of **P1**$_{xy}$, and the characteristic stretching vibrations of Si−O−Si at 1120 cm^{-1}, along with *C*═O vibration absorption band at ∼1706 cm^{-1} still emerges in the in the IR spectrum of **P1$_{xy}$**, confirming that the hydrosilylation reaction was effectively actualized.[40] Simultaneously, the relative intensity of Si−H stretching band at ∼2254 cm^{-1} (vs *C*═O absorption band at ca. ∼1706 cm^{-1}) in the spectra of resulting hybrids obviously decreases with increase of feed ratio of bis-allyoxy monomer to POSS, implying that the number of substituent arms on POSS molecules increases with increasing the feed ratio and the molecular structure of the hybrid composites can be controlled by the changing stoichiometry.

Figure 2 shows the ^{1}H NMR spectra of **M1**, **T$_8^H$**, and **P1**$_{xy}$ hybrids. Obviously, the characteristic olefin proton absorptions located at δ 5.31, 5.35, and 6.01 ppm in the spectrum of **M1** completely disappear after hydrosilylative addition reaction and new broad vibration bands at δ 0.67 (CH_2CH_3CHSi) and 1.25 ppm (CH_2CH_3CHSi) besides 0.86 (CH_2CH_2Si) and 1.85 ppm (CH_2CH_2Si) characteristic absorption band also exist in the spectra of all resulting **P1** hybrids, indicating that the hydrosilylative addition reaction between bis-allyoxy monomers reacting and **T$_8^H$** gave both α- and β-addition isomers at the same time. On the basis of the ratio of the integrated areas of the absorption peaks in the ^{1}H NMR spectra, the proportion of the α- and β-adduct products can be estimated. The results were summarized in Table 1. It can be seen from Table 1 that the α-adduct isomers are the main products when the feed ratio of diene monomer to **T$_8^H$** is at 1:2. However, the proportion of the β-adduct raises significantly and become predominant with further increasing the molar ratio of the diene monomer to POSS such as 1:1 or 2:1, which is significantly different from that reported by Knischka,[41] which the β-adduct increases with decrease of concentrations of the allyl-terminated educts. Simultaneously, based on integrated area of ^{1}H NMR spectra, the average number of substituent group of POSS can be calculated. The results are summarized in Table 1. It can be seen that the average reacted number of Si−H of POSS is about 1 when the feed ratio is 2:1, exhibiting that the resultant hybrid composites may mainly consist of dumbbell-type structural molecules. The average reacted

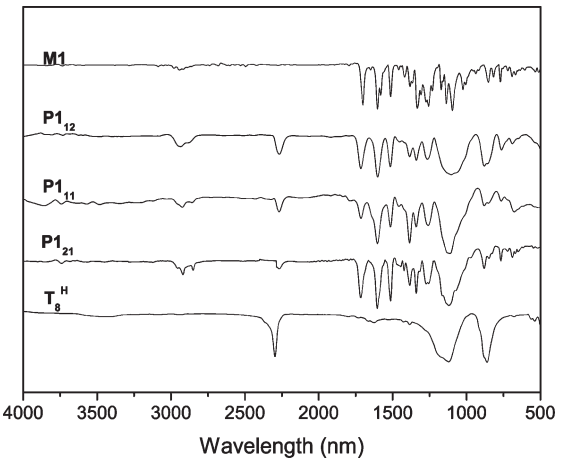

Figure 1. IR spectra of **M1**, **P1$_{12}$**, **P1$_{11}$**, **P1$_{21}$**, and **T$_8^H$**.

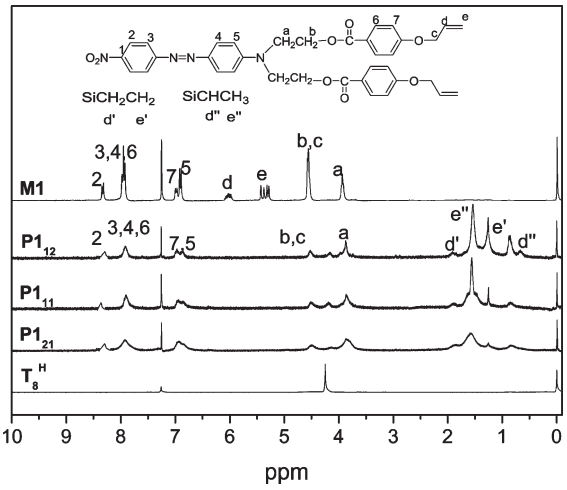

Figure 2. ^{1}H NMR spectra of **M1**, **P1$_{12}$**, **P1$_{11}$**, **P1$_{21}$**, and **T$_8^H$**.

Table 1. Effect of the Feed Ratio on the Properties of the POSS-Based Hybrid Materials

			m^a		
sample	M/T$_8^H$ (molar ratio)	α/β adduct	^{1}H NMR	^{29}Si NMR	T_d (°C)
P1$_{12}$	1:2	63:47	1.16	1.13	334.1
P1$_{11}$	1:1	32:78	1.97	1.92	349.7
P1$_{21}$	2:1	20:80	3.78	3.90	335.3
P2$_{12}$	1:2	65:35	1.72	1.81	349.8
P2$_{11}$	1:1	38:72	1.97	2.05	355.0
P2$_{21}$	2:1	23:77	3.96	4.02	351.4
P3$_{12}$	1:2	60:40	1.13	1.12	349.2
P3$_{11}$	1:1	30:70	2.00	2.16	360.3
P3$_{21}$	2:1	22:78	4.00	4.10	350.0

[a] The average number of reacted Si−H bonds of one POSS molecule.

number of Si−H of POSS is ca. 2 when the feed ratio is 1:1, suggesting that the resulting hybrids composites mainly consist of bead-type structural hybrid molecules. The cross-linked structural hybrid composites are yielded at higher feed ratio, which is almost consistent with that obtained from GPC, further implying that the hydrosilylative addition reaction is carried out at a near stoichiometric ratio.

The cross-polarization method was performed to obtain ^{29}Si MAS NMR spectra. The ^{29}Si NMR spectra of these hybrids also show two resonance absorption peaks at ∼−65.1 and −83.3 ppm, which are attributed to Si resonance absorption of Si−C and unreacted Si−H, respectively, indicative of the formation of the hybrids. This is consistent with the results of IR and ^{1}H NMR spectra. On the basis of the integrations for solid-state ^{29}Si NMR spectra, the average number of substituent group of POSS can also be calculated using the following formula and the results were summarized in Table 1.

$$m = \frac{A_{\mathrm{Si-C}}}{A_{\mathrm{Si-H}} + A_{\mathrm{Si-C}}} \times 8 \qquad (1)$$

Here, A represents the absorbance peak area in the ^{29}Si NMR spectra of the hybrid composites. The values of m obtained by ^{29}Si NMR spectra are almost consistent with that from ^{1}H NMR spectra (Table 1), further supporting that the molecular structure of hybrid composites can be effectively constructed and adjusted by varying the feed ratio of hydrosilylative addition reaction. Simultaneously, it is found that all the hybrids show very good film-forming ability.

UV−Vis Absorption Spectra of Hybrids. The typical UV−vis absorption spectra of the **P1$_{11}$**, **P2$_{11}$**, **P3$_{11}$**, **P1$_{12}$**, **P1$_{21}$**, and **M1** in extremely diluted THF solution (6×10^{-4} g /mL) are shown in Figure 3. It can be seen from Figure 3 that the maximum absorption wavelengths of **P1$_{11}$**, **P2$_{11}$**, and **P3$_{11}$** located at 464, 406, and 408 nm, respectively, which are assigned to the $\pi-\pi^*$ electronic transitions of the corresponding conjugated azobenzene chromophores. Obviously, the maximum absorption wavelengths of the hybrids changes at the different terminal substituents. The absorption peak of the nitro-substituted hybrid **P1$_{11}$** shows significantly red-shifts, which results from the larger π-electron delocalization and stronger dipolar effect of NO_2 group. From Figure 3 it can also be seen that the maximum absorption wavelengths and spectral patterns of the hybrids from different feed ratio and corresponding monomer **M1** (see the spectra of **P1$_{12}$**, **P1$_{11}$**, and **P1$_{21}$**) are nearly same. Similar results are also found in the spectra of **P2$_{xy}$** and **P3$_{xy}$**. Thus, incorporation the POSS cage into the NLO chromophores has little effect on the electronic structures of the free chromophores, although they possess different molecular architecture such as dumbbell-type, bead-type or network-type or cross-liked structures.[42,43] It is noteworthy that the relative absorption intensity of the hybrids increases with the increase of chromophore content in hybrid molecules.

Thermal Stability. Thermal stability of the optical materials is one of the most important aspects to improve device lifetime and reliability. The thermal stability of the resulting hybrids was evaluated by thermogravimetric analysis (TGA) under nitrogen atmosphere. Figure 4 depicts the TGA curves of typical monomer (**M1**) and hybrids (**P1$_{xy}$**) under nitrogen at a heating rate of 10 °C·min^{-1} and the data are summarized in Table 1. The thermal decomposition temperatures (T_d, 5 wt % loss) of organic monomers (**M1**−**M3**) are of 269.4, 271.5, and 275.5 °C, respectively. However, the T_ds of these hybrids are elevated by 64.7−84.5 °C in comparison

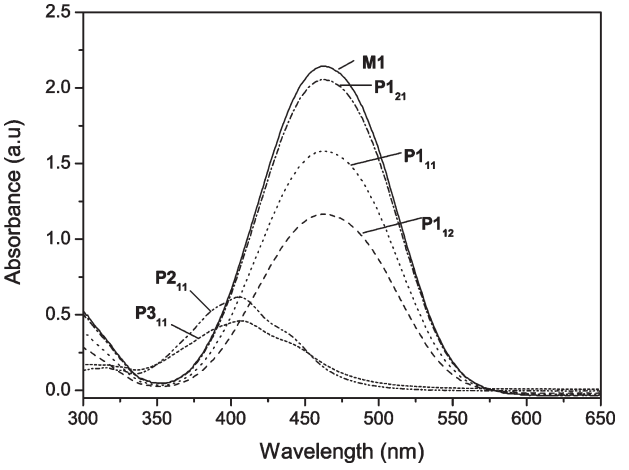

Figure 3. UV−vis absorption spectra of **M1**, **P1$_{12}$**, **P2$_{12}$**, **P3$_{12}$**, **P1$_{11}$**, and **P1$_{21}$** in diluted THF solution (6×10^{-4} g /mL).

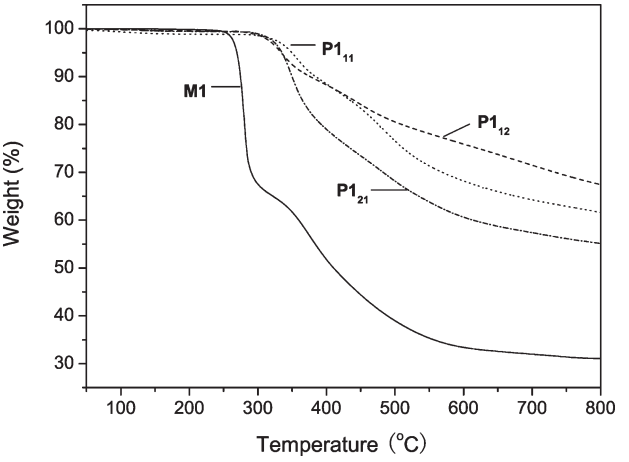

Figure 4. TGA thermograms of **M1**, **P1$_{12}$**, **P1$_{11}$**, and **P1$_{21}$** at a ramp rate of 10 °C/min in nitrogen flow.

with those of the corresponding organic monomers, displaying that the incorporation of the inorganic silsesquioxane core (POSS) into organic NLO chromophores effectively enhances the thermal stability of these resulting functional hybrids. The enhancement of thermal stability may be attributed to the barrier effect of inorganic POSS by limiting heat transfer, which protects the underlying material from heat attack. Simultaneously, the vibration hindrance of organic segments connected covalently to nanosized bulky POSS is also an important factor to result in the thermal stabilizing effect.[44,45] Simultaneously, it is also found that nitro-substituted hybrids show the lowest T_ds, which may be attributed to the larger polarity of nitro group. More interestingly, it is found from Table 1 and Figure 4 that the hybrid molecules (**Pn_{11}**) with bead-type architecture exhibits higher thermal stability than dumbbell-type (**Pn_{12}**) and network-type (**Pn_{21}**) structure. This may be attributed to the "jacket effect" from more regularly arrangement of linear structure, which shields the hybrids from thermal attack and result in the enhancement of thermal performance. Similar phenomenon was also found by our previous work.[46−48]

Nonlinear Optical Properties of Hybrids. The NLO properties of the monomers and hybrids were investigated by using the Z-scan technique.[39] It can be seen from Figure 3 that all the composites have low absorbance at 532 nm. This promises low intensity loss and little temperature change by photon absorption during the NLO measurements. The

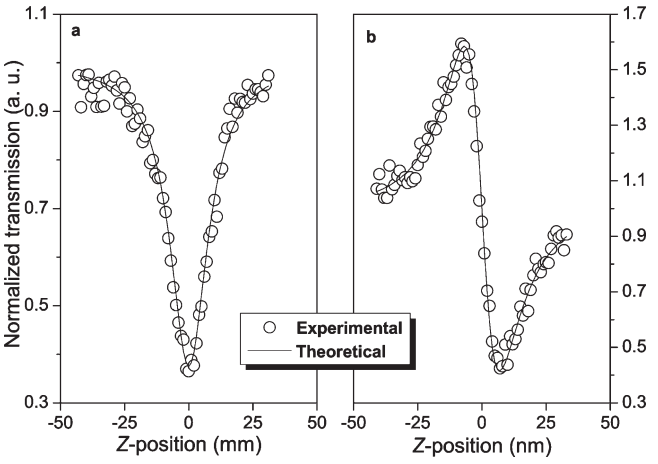

Figure 5. Z scan data of **P1$_{21}$** in THF.

results of Z-scan with and without an aperture show that the nitro-containing monomer and hybrids have both nonlinear absorption and nonlinear refraction, while those monomers and hybrids with methoxyl substituted group and without substituted group exhibit only nonlinear refractions.

The nonlinear absorption coefficient β of the hybrids can be determined through the fitting of the experimental data based on eqs 2 and 3.[39]

$$T(z, s = 1) = \sum_{m=0}^{\infty} \frac{[-q_0(z)]^m}{(m+1)^{3/2}}, \quad \text{for } |q_0| < 1 \qquad (2)$$

$$q_0(z) = \beta I_0(t) L_{\text{eff}}/(1 + Z^2/{Z_0}^2) \qquad (3)$$

Here β is the nonlinear absorption coefficient, $I_0(t)$ the intensity of laser beam at focus ($z = 0$), $L_{\text{eff}} = [1 - \exp(-\alpha_0 L)/\alpha_0$ is the effective thickness with α_0 the linear absorption coefficient and L the sample thickness, z_0 is the diffraction length of the beam, and z is the sample position. The solid line in Figure 5a is theoretical curve from eqs 2 and 3. Thus, β of the hybrid can be determined through the fitting of the experimental data with the equations.

The nonlinear refractive coefficient (n_2) of the hybrids can be determined by fitting the experimental data (Figure 5b) using eq 4.[39,49]

$$T(z, \Delta\phi) = 1 + \frac{4\Delta\phi x}{(x^2 + 9)(x^2 + 1)} \qquad (4)$$

Here $x = z/z_0$ and $\Delta\phi$ is on-axis phase change caused by the nonlinear refractive index of the sample and $\Delta\phi = 2\pi I_0 (1 - e^{-\alpha L}) n_2/\lambda\alpha_0$.

In accordance with the observed β and n_2 values, the third-order susceptibility $\chi^{(3)}$ value can be calculated with the following equation:

$$|\chi^{(3)}| = \sqrt{\left|\frac{c{n_0}^2}{80\pi} n_2\right|^2 + \left|\frac{9 \times 10^8 \varepsilon_0 {n_0}^2 c^2}{4\pi\omega}\beta\right|^2} \qquad (5)$$

Here ε_0 is the permittivity of vacuum, c the speed of light, and n_0 the refractive index of the medium, and $\omega = 2\pi c/\lambda$.

The nonlinear optical coefficients of the monomers and these hybrids (**Px_{11}**) at concentration 1 mg/mL in THF solution are summarized in Table 2. From Table 2 it can be seen that the hybrids exhibit slightly lowered $\chi^{(3)}$ value in comparison with their corresponding monomers, which result from the lower chromophoric content in unit volume due to the introduction of bulk POSS cages. In addition, we can also found that the nitro-containing hybrids showed lager $\chi^{(3)}$ value than those hybrids with methoxyl group or without substituted group, due to the larger π-electron delocalized and dipolar effect, which is consistent with the results of UV spectra.

Table 2. Nonlinear Optical Properties of Monomers and Hybrids in 1 mg/mL THF Solutions

	NLO properties[a]		
sample	β (m/W)	n_2 (m^2/W)	$\chi^{(3)}$ (esu)
M1	0.57×10^{-10}	8.24×10^{-18}	1.95×10^{-11}
P1$_{11}$		6.08×10^{-18}	1.44×10^{-11}
M2		0.84×10^{-18}	1.97×10^{-12}
P2$_{11}$		0.83×10^{-18}	1.95×10^{-12}
M3		0.64×10^{-18}	1.51×10^{-12}
P3$_{11}$		0.61×10^{-18}	1.44×10^{-12}

[a] Measured by the Z-scan technique with a 13 ns Nd:YAG laser system at a 1 Hz repetition rate and 532 nm wavelength.

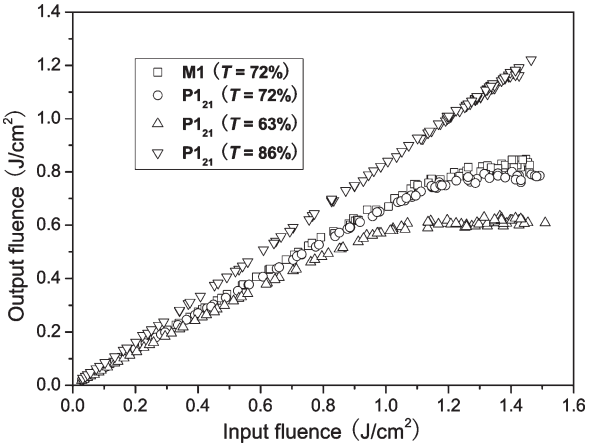

Figure 6. Optical responses to laser light of **M1** with a linear transmission of 72% and **P1$_{21}$** with different linear transmittances in THF.

Optical Limiting Properties. Figure 6 shows the example OL performances of **P1$_{21}$** (concentration $c = 0.87$ mg/mL) and **M1** ($c = 0.35$ mg/mL) at the same linear transmittance ($T = 72\%$) to 532 nm laser pulses in THF. At low incident energies the optical responses follow Beer's law. Deviations from Beer's law at higher energies indicate the occurrence of optical limiting. Experiments with THF solvent alone afforded no detectable OL effect. This indicates that the solvent contribution is negligible. As seen from Figure 6, **M1** and **P1$_{21}$** show nearly the same limiting threshold (incident fluence at which the output fluence starts to deviate from linearity) and amplitude (maximum output fluence), which are 0.68 and 0.83 J/cm^2, respectively, indicating the introduction of the POSS cage shows little effect on the OL properties of the resulting hybrids, which is consistent with phenomenon observed in UV spectra. Simultaneously, the OL results of **P1$_{21}$** solutions at 86% and 63% transmittances are also displayed in Figure 6. It can be seen that the OL effect increases with the decrease of the transmittance. For example, **P1$_{21}$** solution at 86% transmittance shows no obvious OL performance. When the transmittance decreased from 72% to 63%, the limiting threshold of the sample varied from 0.68 to 0.40 J/cm^2 and the limiting amplitude varied from 0.59 to 0.64 J/cm^2, respectively. Similar results were also found in our previous work.[49,50] It is the reason that the solution with a low transmittance (high

concentration) has more molecules per unit volume, which should absorb the energy of the harsh laser more efficiently. We also measured the UV absorption spectrum of the hybrid solutions before and after the laser irradiation and found that the pattern and intensity of their UV absorption spectra have almost no change, hinting that the hybrids possess well photostability.

Conclusions

In this work, series of POSS-based azobenzene-containing inorganic−organic functional hybrid materials with different architecture, such as dumbbell-type, line-type and cross-linked structure were prepared via the hydrosilylative reaction by varying the feed ratio. It is found that both α and β adducts were observed in the hybrids and the proportion of β adducts was significantly affected by feed ratio and molecular structure of reacted organic monomer, and increased with increasing feed ratio of bis-allyoxy monomer. The incorporation of inorganic POSS cage into NLO chromophores not only retained the NLO and OL properties of the chromophores, but also endows the hybrids with better solubility and well film-forming ability, as well as significant enhanced thermal stability. The work provides a novel path for design and preparation of new NLO hybrid materials.

Acknowledgment. This research was financially supported by the National Natural Science Fund of China (Grant Nos. 90606011, 50472038 and 20974018), Ph.D. Program Foundation of Ministry of Education of China (No.20070255012), Shanghai Leading Academic Discipline Project (No. B603) and Open Project of The State Key Laboratory of Crystal Materials (KF0809), the Program of Introducing Talents of Discipline to Universities (No.111-2-04) and China Postdoctoral Science Foundation (20080440563).

References and Notes

(1) Ehrlich, J. E.; Wu, X. L.; Lee, I.-Y. S.; Hu, Z.-Y.; Röckel, H.; Marder, S. R.; Perry, J. W. *Opt. Lett.* **1997**, *22*, 1843–1845.
(2) Guang, S.; Yin, S.; Xu, H.; Zhu, W.; Gao, Y.; Song, Y. *Dyes Pigm.* **2007**, *73*, 285–291.
(3) Tutt, L. W.; Kost, A. *Nature* **1992**, *356*, 225.
(4) de la Torre, G.; Claessens, C. G.; Torres, T. *Chem. Commun.* **2007**, 2000–2015.
(5) Chen, Y.; O'Flaherty, S.; Fujitsuka, M.; Hanack, M.; Subramanian, L. R.; Ito, O.; Blau, W. J. *Chem. Mater.* **2002**, *14*, 5163–5168.
(6) McEwan, K.; Lewis, K.; Yang, G.-Y.; Chng, L.-L.; Lee, Y.-W.; Lau, W.-P.; Lai, K.-S. *Adv. Funct. Mater.* **2003**, *13*, 863–867.
(7) Pittman, M.; Plaza, P.; Martin, M. M.; Meyer, Y. H. *Opt. Commun.* **1998**, *158*, 201–212.
(8) Manners, I. *Science* **2001**, *294*, 1664–1666.
(9) Mather, P. T.; Jeon, H. G.; Romo-Uribe, A.; Haddad, T. S.; Lichtenhan, J. D. *Macromolecules* **1999**, *32*, 1194–1203.
(10) Xu, H.; Yang, B.; Wang, J.; Guang, S.; Li, C. *Macromolecules* **2005**, *38*, 10455–10460.
(11) Baney, R. H.; Itoh, M.; Sakakibara, A.; Suzuki, T. *Chem. Rev.* **1995**, *95*, 1409–1430.
(12) Feng, Y.; Jia, Y.; Xu, H. Y. *J. Appl. Polym. Sci.* **2009**, *111*, 2684–2690.
(13) Maitra, P.; Wunder, S. L. *Chem. Mater.* **2002**, *14*, 4494–4497.
(14) Haddad, T. S.; Lichtenhan, J. D. *Macromolecules* **1996**, *29*, 7302–7304.
(15) Lichtenhan, J. D.; Otonari, Y. A.; Carr, M. J. *Macromolecules* **1995**, *28*, 8435–8437.
(16) Yang, B. H.; Li, J. R.; Wang, J. F.; Xu, H. Y.; Guang, S. Y.; Li, C. *J. Appl. Polym. Sci.* **2009**, *111*, 2963–2969.
(17) Kulkarni, A. P.; Jenekhe, S. A. *Macromolecules* **2003**, *36*, 5285–5296.
(18) Liu, Y. L.; Fangchiang, M. H. *J. Mater. Chem.* **2009**, *19*, 3643–3647.
(19) Zhang, C.; Bunning, T. J.; Laine, R. M. *Chem. Mater.* **2001**, *13*, 3653–3662.
(20) Pan, Q.; Chen, X.; Fan, X.; Shen, Z.; Zhou, Q. *J. Mater. Chem.* **2008**, *18*, 3481–3488.
(21) Chen, K.-B.; Chang, Y.-P.; Yang, S.-H.; Hsu, C.-S. *Thin Solid Films* **2006**, *514*, 103–109.
(22) Lo, M. Y.; Zhen, C.; Lauters, M.; Jabbour, G. E.; Sellinger, A. *J. Am. Chem. Soc.* **2007**, *129*, 5808–5809.
(23) Xiao, Y.; Liu, L.; He, C.; Chin, W. S.; Lin, T.; Mya, K. Y.; Huang, J.; Lu, X. *J. Mater. Chem.* **2006**, *16*, 829–836.
(24) Imae, I.; Kawakami, Y. *J. Mater. Chem.* **2005**, *15*, 4581–4583.
(25) Lo, M. Y.; Ueno, K.; Tanabe, H.; Sellinger, A. *Chem. Rec.* **2006**, *6*, 157–168.
(26) Miyake, J.; Chujo, Y. *Macromol. Rapid Commun.* **2008**, *29*, 86–92.
(27) Soh, M. S.; Yap, A. U. J.; Sellinger, A. *Eur. Polym. J.* **2007**, *43*, 315–327.
(28) Knight, P. T.; Lee, K. M.; Qin, H.; Mather, P. T. *Biomacromolecules* **2008**, *9*, 2458–2467.
(29) Xu, H.; Yang, B.; Wang, J.; Guang, S.; Li, C. *J. Polym. Sci., Part A: Polym. Chem.* **2007**, *45*, 5308–5317.
(30) Yang, B.; Xu, H.; Wang, J.; Gang, S.; Li, C. *J. Appl. Polym. Sci.* **2007**, *106*, 320–326.
(31) Xu, H.; Yang, B.; Gao, X.; Li, C.; Guang, S. *J. Appl. Polym. Sci.* **2006**, *101*, 3730–3735.
(32) Xu, H. Y.; Yang, B. H.; Wang, J. F.; Guang, S. Y.; Li, C. *Macromolecules* **2005**, *38*, 10455–10460.
(33) Ceyhan, T.; Yüksek, M.; Yağlıoğlu, H. G.; Salih, B.; Erbil, M. K.; Elmalí, A.; Bekaroğlu, Ö. *Dalton Trans.* **2008**, 2407–2413.
(34) Su, X.; Xu, H.; Deng, Y.; Li, J.; Zhang, W.; Wang, P. *Mater. Lett.* **2008**, *62*, 3818–3820.
(35) Agaskar, P. A. *J. Am. Chem. Soc.* **1989**, *111*, 6858–6859.
(36) Apfel, M. A.; Finkelmann, H.; Janini, G. M.; Laub, R. J.; Luehmann, B. H.; Price, A.; Roberts, W. L.; Shaw, T. J.; Smith, C. A. *Anal. Chem.* **1985**, *57*, 651–658.
(37) Choi, J.; Harcup, J.; Yee, A. F.; Zhu, Q.; Laine, R. M. *J. Am. Chem. Soc.* **2001**, *123*, 11420–11430.
(38) Qu, S.; Song, Y.; Du, C.; Wang, Y.; Gao, Y.; Liu, S.; Li, Y.; Zhu, D. *Opt. Commun.* **2001**, *196*, 317–323.
(39) Sheik-Bahae, M.; Said, A. A.; Wei, T.-H.; Hagan, D. J.; Stryland, E. W. V. *IEEE J. Quantum Electron.* **1990**, *26*, 760–769.
(40) Zhang, C.; Laine, R. M. *J. Am. Chem. Soc.* **2000**, *122*, 6979–6988.
(41) Knischka, R.; Dietsche, F.; Hanselmann, R.; Frey, H.; Mülhaupt, R. *Langmuir* **1999**, *15*, 4752–4756.
(42) Sung, H.-H.; Lin, H.-C. *Macromolecules* **2004**, *37*, 7945–7954.
(43) Xiao, S.; Nguyen, M.; Gong, X.; Cao, Y.; Wu, H.; Moses, D.; Heeger, A. J. *Adv. Funct. Mater.* **2003**, *13*, 25–29.
(44) Asuncion, M. Z.; Laine, R. M. *Macromolecules* **2007**, *40*, 555–562.
(45) Markovic, E.; Matisons, J.; Hussain, M.; Simon, G. P. *Macromolecules* **2007**, *40*, 2694–2701.
(46) Su, X.; Xu, H.; Guo, Q.; Shi, G.; Yang, J.; Song, Y.; Liu, X. *J. Polym. Sci., Part A: Polym. Chem.* **2008**, *46*, 4529–4541.
(47) Su, X.; Xu, H.; Yang, J.; Lin, N.; Song, Y. *Polymer* **2008**, *49*, 3722–3730.
(48) Wang, X.; Guang, S.; Xu, H.; Su, X.; Yang, J.; Song, Y.; Lin, N.; Liu, X. *J. Mater. Chem.* **2008**, *18*, 4202–4209.
(49) Yin, S. C.; Xu, H. Y.; Su, X. Y.; Li, G.; Song, Y. L.; Lam, J. W. Y.; Tang, B. Z. *J. Polym. Sci., Part A: Polym. Chem.* **2006**, *44*, 2346–2357.
(50) Su, X.; Wu, L.; Yin, S.; Xu, H.; Wu, Z.; Song, Y.; Tang, B. Z. *J. Macromol. Sci., Pure Appl. Chem.* **2007**, *44*, 691–697.